

DAΦNE & KLOE-2

Antonio De Santis[‡]

INFN - Laboratori Nazionali di Frascati, v. Enrico Fermi, 50, 00044

E-mail: antonio.desantis@lnf.infn.it

February 2015

Abstract. The DAΦNE collider, located in the Frascati National Laboratories of INFN, has two main rings, where electrons and positrons are stored to collide at a center of mass energy of 1.02 GeV, the ϕ resonance mass. KLOE-2 experiment is located at the collider interaction region. The detector is capable to observe and collect data coming from ϕ decay: charged and neutral kaon pairs, lighter unflavored mesons (η , η' , f_0 , a_0 , ω/ρ).

In the first half of 2013 the KLOE detector has been upgraded inserting new detector layers in the inner part of the apparatus, around the interaction region in order to improve detector hermeticity and acceptance. The long shutdown has been used to undertake a general consolidation program aimed at improving the DAΦNE performances.

This contribution presents the ϕ -factory setup and the achieved performances in terms of beam currents, luminosity and related aspects together with the KLOE-2 physics program, upgrade status report and recent physics results.

1. DAΦNE preparation for KLOE-2 physics run

DAΦNE [1] is a double ring lepton collider working at the Φ -resonance c.m. energy (1.02 GeV). The two rings layout crosses two times, but the vacuum chamber is shaped in a such way that only one Interaction Region (IR) is possible where the KLOE-2 detector is currently installed. The complex includes a S-band linac, 180 m long transfer lines and an accumulator/damping ring, providing fast and high efficiency top-up electron/positron injection. DAΦNE reached its maximum luminosity during the test of the new Crab-Waist (CW) collision scheme [2] achieving a peak luminosity, $L = 4.5 \times 10^{32} \text{cm}^{-2} \text{s}^{-1}$, two orders of magnitude higher than the one measured by other colliders working at the same c.m. energy.

The new IR [3] for the KLOE-2 experiment with CW has been designed, installed and tested already

[‡] on behalf of KLOE-2 Collaboration and DAΦNE team: D. Alesini, M.E. Biagini, S. Bini, M. Boscolo, B. Buonomo, S. Cantarella, G. Di Pirro, G. Delle Monache, A. Drago, L. Foggetta, O. Frasciello, A. Gallo, A. Ghigo, S. Guiducci, C. Ligi, G. Mazzitelli, C. Milardi, L. Pellegrino, R. Ricci, U. Rotundo, C. Sanelli, M. Serio, A. Stella, A. Stecchi, M. Zobov, LNF-INFN, Frascati, Italy.

in the 2010-2012 reaching a instantaneous luminosity of $L = 1.52 \times 10^{32} \text{cm}^{-2} \text{s}^{-1}$ [4]. During the first seven months of 2013, the accelerator complex has been shut-down again mainly to install KLOE-2 detector upgrade [5] and to implement a general consolidation program concerning several machine subsystems [6, 7]. Such upgrade imposed the extraction of the IR from inside the detector and the disassembly of the low- β section thus implying new commissioning [8].

During the test run of 2012, the mechanical structure of the IR had shown to be inadequate to steadily support the heavy defocusing quadrupoles cantilevered inside the detector. As a consequence, the two beams were oscillating in phase at 10 Hz in the vertical plane, as shown in fig. 1. Moreover some components got seriously damaged: some bellows in the IR, which had lost electrical continuity causing anomalous beam induced heating of one of the two defocusing quadrupoles, resulting in a harmful random vertical tune-shift.

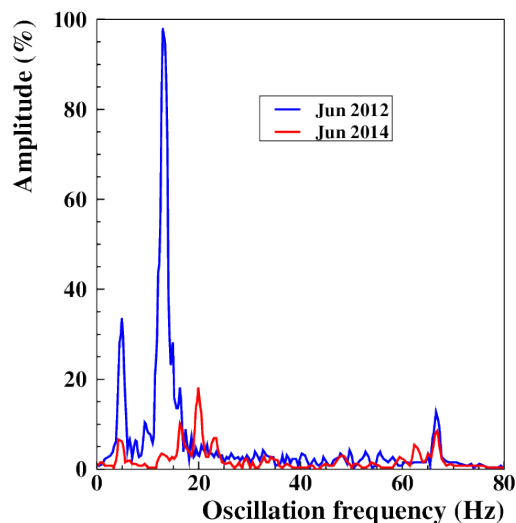


Figure 1. IR mechanical vibration spectrum. Darker line is for the new supporting structure.

The vacuum chamber around the Interaction Point (IP) has been replaced. The new one has tapered transition between the thin ALBEMET sphere and the Al beam pipes, and includes reshaped bellows with new designed RF contacts. Replacing the bellows solved the low- β defocusing quadrupole heating problems, recovering working point stability in operations.

Two cooling pipes have been added on the tapers and new semi-cylindrical thin ($35 \mu\text{m}$) beryllium shields have been placed inside the sphere. Two additional Beam Position Monitors (BPM) have been installed on both sides of the IP, for a more accurate beams overlap and to perform transverse betatron coupling studies.

During the DAΦNE long standing history the high positron current regime was always characterized by instabilities induced by the electron cloud. During the test run of 2012 special electrodes [9] inside dipoles and wigglers vacuum chambers were installed to mitigate the effect. Several measurements and tests demonstrated their effectiveness in thwarting the e-cloud [10]. These first studies have all been done by polarizing the strip-line with a positive voltage in the range 0-250 V while simulations indicate that a factor two higher voltage is required to completely neutralize the e-cloud density due to a positron current of the order of 1 A. For this reason during the 2013 shutdown the electrode power supplies have been replaced with devices providing a maximum negative voltage of 500 V. The change of polarity was intended to limit the current delivered by the power supplies.

2. DAΦNE commissioning

DAΦNE operation started by the end of January 2014, but it has been severely slowed down by three main interruptions due to external circumstances that imposed two and a half months of inactivity.

The betatron tunes working points adopted by now are: $\nu_x^- = 5.098$, $\nu_y^- = 5.164$ and $\nu_x^+ = 5.1023$, $\nu_y^+ = 5.139$, which, according LIFETRAC [11] simulations should provide good luminosity and lay in a rather large stable area still to be explored.

Transverse betatron coupling has been optimized by tuning the rotations of the low- β focusing quadrupoles. Presently a very good coupling correction has been achieved for the positron beam, $\kappa \sim 0.4\%$, without skew quadrupoles, while a further optimization is needed for the electron beam. Tuning the skew quadrupoles a transverse betatron coupling of 0.2%-0.3% has been achieved in both rings.

Machine operation at high current strongly depends on vacuum conditions. Since the beam pipe has been opened in several main ring sections, a quite long time has been spent to recover a reasonable dynamic vacuum level. Highest currents stored, so far, in 98 contiguous bunches are 1.7 A and 1.15 A, for electron and positron beam, respectively. These currents are the highest ever achieved after installing the new IR for the KLOE-2 detector, based on the CW collision scheme. To reach such high current the three independent bunch-by-bunch feedback systems [12] installed on each DAΦNE ring are essential. The positron vertical feedback is now using a new ultra-low noise front-end module, designed in collaboration with the SuperKEKB feedback team.

Presently beam dynamics in the positron ring is clearly dominated by the electron-cloud induced instabilities. To cope with these effects several system

are used: bunch-by-bunch transverse feedback systems, solenoids wound all around the straight sections and on-purpose designed electrodes [9] installed inside dipole and wiggler vacuum chambers. The new setup of electrodes, described in the previous section, has been tested storing a ~ 700 mA current in 90 bunches spaced by 2.7 ns, and measuring the horizontal and vertical tune spread along the batch with the electrodes on and off. Results show a clear reduction of the tune spread in both planes, but especially in the horizontal one [13].

Another positive result in mitigating the detrimental effects induced by the e-cloud has been obtained lengthening the bunch by reducing the voltage of the RF cavity of the positron ring, as shown in fig. 2, where the dynamic vacuum condition is shown as a function of the beam current for different High Voltage sets of the RF cavity.

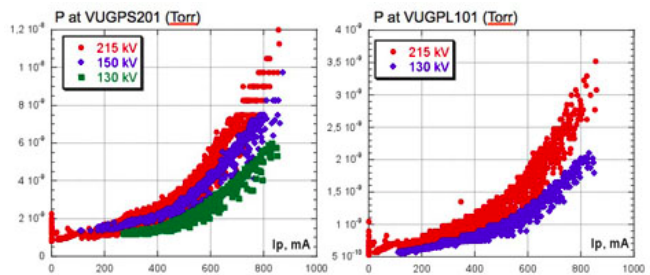


Figure 2. Variation of the vacuum pressure in the arcs as a function of RF cavity voltage. The reduction of RF High Voltage results in a slower growth of the dynamical vacuum pressure because the induced lengthening of the beam bunch reduces the charge density with same total beam current and thus the e-cloud acceleration towards the beam line is weaker.

Collisions has been optimized without the CW Sextupoles. The overlap between colliding beams has been recovered, both in transverse and longitudinal plan, taking advantage from the two new beam position monitors installed around the IP. The highest luminosity measured in large Piwinsky angle regime without the CW Sextupoles has been slightly in excess of $10^{32}\text{cm}^{-2}\text{s}^{-1}$. In this configuration several effects have been observed such as: considerable reduction of the lifetime of one beam when injecting the other, transverse beam blow-up at high currents and deleterious background level. These phenomena are correlated to the synchro-betatron resonances affecting collisions in large Piwinsky angle regime. The CW Sextupoles have been aligned on the collision orbit, by using beam based alignment techniques, and their field increased progressively, while tuning collisions, till reaching strengths of the order of 70% and 50% of the nominal ones for positron and electron, respectively. The reduction of the vertical beam size, as seen on the synchrotron light monitor, is shown in fig. 3.

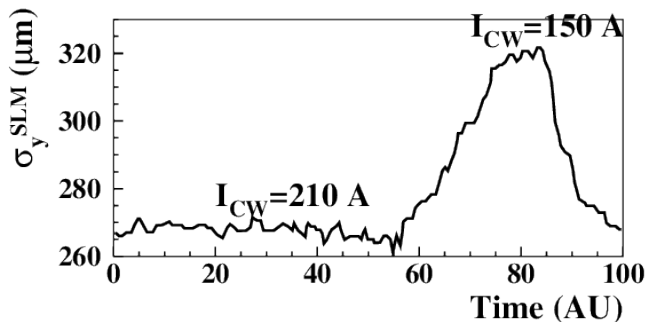


Figure 3. Effect of the CW sextupoles on the transverse dimensions of the positron beam. When the CW sextupole current is lowered from 210 A to 150 A, a sizeable growth of vertical beam size is observed at the Synchrotron Light Monitor from 265 μm to 320 μm .

The increase of bunch length, useful for mitigating the electron cloud effect on the positron beam, for both beams appreciably contributed in enhancing peak luminosity. The convoluted vertical sizes of the colliding bunches as measured by beam-beam scan at low current is $\sigma_y = 5.4\mu\text{m}$, due to the not yet optimized transverse coupling in the electron beam. The highest luminosity attained, so far, is $L = 1.71 \times 10^{32} \text{cm}^{-2}\text{s}^{-1}$ measured with current of the order of $I^- \sim 0.96$ A and $I^+ \sim 0.89$ A stored in 100 bunches. This value exceeds by a 13% the best luminosity ever achieved, at DAΦNE during operations with KLOE detector.

Instantaneous luminosity in the present DAΦNE configuration is measured by the KLOE-2 detector every 30 seconds. A faster monitor measures the photon emitted at small angle (~ 1 mrad) in the e^+e^- inelastic scattering and is used only for relative luminosity measurements, during collision optimization.

Furthermore a rather promising hourly integrated luminosity has been recorded averaging over two hours, in moderate injection regime: $\int_{1h} L \sim 0.4 \text{ pb}^{-1}$, see fig. 4 This measurement indicates that, having a reasonable up-time, a daily integrated luminosity at least of the order of $\sim 10\text{pb}^{-1}$ can be delivered to the experiment.

3. KLOE-2 experimental apparatus

The KLOE-2 experiment is an upgraded version of the old KLOE apparatus with the inclusion of new sub-detectors allowing for larger physics program with increased reconstruction performance.

The original KLOE detector consists of a large cylindrical drift chamber (DC) surrounded by a lead-scintillating fiber electromagnetic calorimeter (EMC). A super-conducting coil around the EMC provides a 0.52 T axial field.

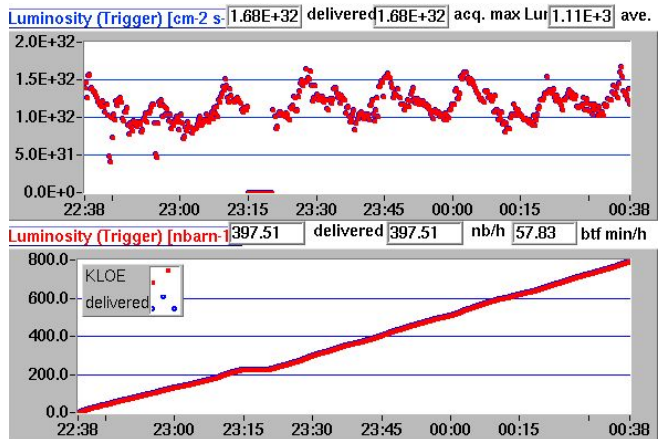


Figure 4. Instantaneous (top) and integrated (bottom) luminosity.

The DC [14] is 4 m in diameter and 3.3 m long and has 12,582 all-stereo cells properly arranged in 58 layers to ensure homogeneous detector response. Time and amplitude of signals from cells are read-out to measure hit positions and energy loss. The chamber structure is made of carbon-fiber epoxy composite and the gas mixture used is 90% helium, 10% isobutane. These features maximize transparency to photons and reduce $K_L \rightarrow K_S$ regeneration and multiple scattering. The position resolutions for single hits are $\sigma_{r,\phi} \sim 150 \mu\text{m}$ and $\sigma_z \sim 2$ mm in the transverse and longitudinal plane, respectively and are almost homogeneous in the active volume. The momentum resolution is $\sigma(p_\perp)/p_\perp \sim 0.4\%$ for polar angles in the range $40^\circ - 130^\circ$.

The EMC [15] is divided into a barrel and two end-caps covering 98% of the solid angle. Signals from impinging particles are read out at both ends of each module by photo-multipliers for a total of 2440 cells arranged in five layers in depth. Amplitudes and time of the signals are recorded. Cells close in time and space are grouped into calorimeter clusters. The cluster energy E_{clu} is the sum of its cell energies. The cluster time T_{clu} and position \vec{R}_{clu} are energy-weighted averages. Energy and time resolutions are $\sigma_E/E_{\text{clu}} = 5.7\%/\sqrt{E_{\text{clu}}(\text{GeV})}$ and $\sigma_{T_{\text{clu}}} = 57\text{ps}/\sqrt{E_{\text{clu}}(\text{GeV})} \oplus 100$ ps, respectively.

The KLOE-2 experimental program [16] implies several detector improvements in order to increase the physics results outcomes. For the gamma-gamma physics two pairs of electron-positron taggers have been installed. A small LYSO crystal calorimeter matrix, the Low Energy Tagger [18] inside KLOE apparatus and a plastic scintillator hodoscope, the High Energy Tagger [19], along the beam lines outside the KLOE detector.

To improve the acceptance and the angular coverage two new calorimeters have been developed. A

pair of LYSO crystal calorimeters (CCALT) [20] have been installed near the interaction region to improve the angular acceptance for low- θ particles. This calorimeter will be also useful to provide fast signals for luminosity measurement and beam instability feedback to help DAFNE tune-up.

A pair of tile calorimeters (QCALT) [21], covers the quadrupoles inside the KLOE detector and along the beam pipe. These calorimeters are made of tungsten slabs and singly read-out scintillator tiles to improve the angular coverage for particles coming from the active volume of the DC (e.g. K_L decay).

In order to increase the resolution on the vertex reconstruction for decay in the vicinity of the primary interaction point a small and light inner tracker (IT) [22] made of four planes of cylindrical GEM has been designed.

During data taking DAΦNE beam conditions and detector calibrations are constantly monitored in order to guarantee the highest quality of the collected data.

4. Physics result with KLOE

4.1. Kaon interferometry

The Φ meson produced at DAΦNE Φ -factory have a small residual momentum in the horizontal plane and the branching fraction for the Φ decay in neutral kaon pair is 34%. This decay, due to strong interaction, preserve parity (P) and charge conjugation (C) eigenvalue of the initial state: $J^{PC} = 1^{--}$. The initial state can be represented as an anti-symmetric combination of the two neutral kaon mass eigenstate:

$$|\Phi\rangle \propto |K_S, \vec{p}\rangle |K_L, -\vec{p}\rangle - |K_S, -\vec{p}\rangle |K_L, \vec{p}\rangle$$

The time evolution of the kaon system preserve the initial correlation even at the kaon decay level. Labelling f_1 and f_2 the final decay channels for the two kaons and evaluating the probability of a decay into $|f_1, f_2\rangle$ final state as a function of the difference of proper decay times ($\Delta\tau = \tau_2 - \tau_1$) the following equation is obtained (For a detailed treatment of quantum interference [23]).

$$I_{f_1 f_2}(\Delta\tau) \propto e^{-\Gamma|\Delta\tau|} \left[|\eta_{f_1}|^2 e^{\frac{\Delta\Gamma}{2}\Delta\tau} + |\eta_{f_2}|^2 e^{-\frac{\Delta\Gamma}{2}\Delta\tau} - 2\Re\left(\eta_{f_1}\eta_{f_2}^* e^{-i\Delta m\Delta\tau}\right) \right] \quad (1)$$

where $\eta_{f_j} = \langle f_j | K_L \rangle / \langle f_j | K_S \rangle$, $\Gamma = \Gamma_S + \Gamma_L$ and $\Delta\Gamma = \Gamma_S - \Gamma_L$.

Eq. 1 shows a time interference term characteristic of the so-called EPR correlation from the names of Einstein, Podolsky and Rosen [24] that firstly pointed out this kind of effect.

In this analysis the final state chosen is $|f_1\rangle = |f_2\rangle = |\pi^+\pi^-\rangle$ and a fully destructive interference is

expected for equal decay times ($|\Delta\tau| = 0$). The ratio of neutral kaon decay amplitudes (η_j) becomes:

$$\eta_j = \eta_{\pi^+\pi^-} = \frac{\langle \pi^+\pi^- | T | K_L \rangle}{\langle \pi^+\pi^- | T | K_S \rangle} \simeq \varepsilon_K + \varepsilon' - \delta_K \quad (2)$$

where ε_K is the CP violation parameter in the mixing, ε' is the direct CP violation parameter and δ_K stands for the amount of CPT violations. In the Standard Model Extension (SME) framework [25], according to Greenberg theorem [26], the δ_K parameter is expected to have the following expression:

$$\delta_K \approx i \sin \phi_{SW} e^{i\phi_{SW}} \gamma_K (\Delta a_0 - \vec{\beta}_K \cdot \Delta \vec{a}) / \Delta m, \quad (3)$$

where γ_K and β_K are the usual Lorentz factors for the kaon, ϕ_{SW} is the super-weak phase and Δa_μ are the SME parameters for the kaon system.

Eq. 3 shows that δ_K is modulated by the kaon momentum modulus (γ_K and $|\vec{\beta}_K|$) and by its spatial direction ($\vec{\beta}_K$). In the KLOE case the two kaons are produced almost back-to-back in the Φ decay and therefore evolve with two different δ_K ($\delta_K(\vec{P}_1) \neq \delta_K(\vec{P}_2)$). Additional angular dependence in the eq. 1 through eq. 3 are induced by the Earth motion (sidereal time variation) and residual Φ momentum in the lab frame. The effect produced by CPT violation can be observed in the distribution of eq. 1 provided that the two kaon final states are tagged with respect to some reference direction in the laboratory frame and taking into account the proper coordinate transformation in the privileged reference frame where eq. 3 holds in this form (see equation 14 of reference [25]). The signal selection starts with the request of two decay vertices with two tracks connected each. The same kinematical selection criteria are requested in order to obtain the cleanest and less biased sample of $K \rightarrow \pi\pi$ possible. At the end of the selection chain the background contamination, according to the MC estimate, is 1.5% and is mainly due to kaon regeneration on the beam pipe structure.

The data distributions have been fitted with the eq. 1 including the SME effects.

The $\Delta\tau$ range is: $\Delta\tau \in [-12 : 12]\tau_S$. This choice is to limit the perturbation on the result by the regeneration on the thicker part of the beam pipe, the Al-Be spherical pipe [27]. The sample of data collected has been splitted in four sidereal time bins and two angular selection for a grand total of 192 experimental points simultaneously used for fitting, as shown in fig. 5

The results for the Δa_μ parameters are [28]:

$$\begin{aligned} \Delta a_0 &= (-6.0 \pm 7.7_{stat} \pm 3.1_{syst}) \times 10^{-18} \text{ GeV}, \\ \Delta a_X &= (0.9 \pm 1.5_{stat} \pm 0.6_{syst}) \times 10^{-18} \text{ GeV}, \\ \Delta a_Y &= (-2.0 \pm 1.5_{stat} \pm 0.5_{syst}) \times 10^{-18} \text{ GeV}, \\ \Delta a_Z &= (3.1 \pm 1.7_{stat} \pm 0.5_{syst}) \times 10^{-18} \text{ GeV}. \end{aligned}$$

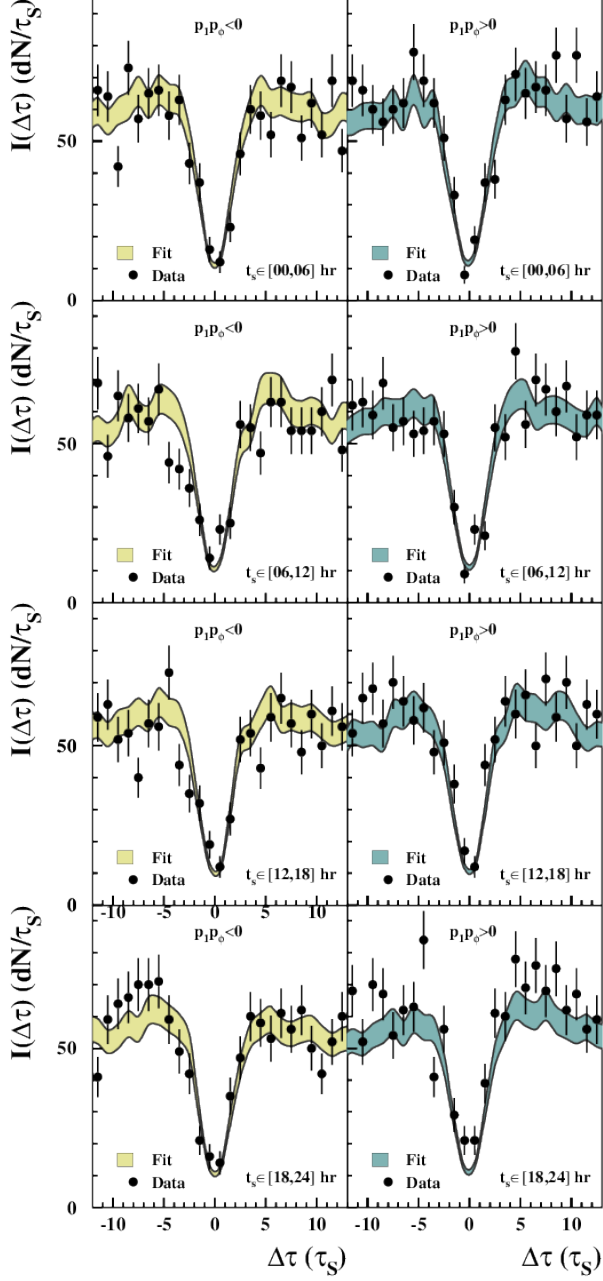


Figure 5. Fit results: the top and bottom plots refer to the two angular selections. Black points are for experimental data while colored bands are the fit output. The error bars on experimental data are purely statistical, while the band represents the contribution to the uncertainty due to MC simulation statistics and efficiency correction. The fit χ^2/N_{DoF} is 211.7/187 corresponding to a probability of 10%.

Which constitute the most precise result in the quark sector of the SME. The total error is fully dominated by the statistical uncertainty.

4.2. $BR(K^+ \rightarrow \pi^+ \pi^- \pi^+ (\gamma))$ measurement

The last measurement of $BR(K^\pm \rightarrow \pi^\pm \pi^+ \pi^-)$ was performed in 1972 without information about the radiation cut-off [29] whereas value reported in PDG [30] is obtained from a global fit that does not use any of the available $BR(K^\pm \rightarrow \pi^\pm \pi^+ \pi^-)$ measurements but the rate measurement $\Gamma(\pi^+ \pi^+ \pi^-) = (4.511 \pm 0.024) \times 10^6 \text{ s}^{-1}$ published in 1970 [31]. In the $\pi^0 \pi^0$ invariant mass distribution of data collected by NA48 a cusp-like anomaly at $M_{00} = 2m_{\pi^+}$ can be observed [32]. The interpretation is the final state charge-exchange reaction $\pi^+ \pi^- \rightarrow \pi^0 \pi^0$ in $K^\pm \rightarrow \pi^\pm \pi^+ \pi^-$ decay [33, 34]. Based on the fit of models [35] and [36, 37] to experimental M_{00}^2 distribution the difference between the S-wave $\pi\pi$ scattering lengths in the isospin $I=0$ and $I=2$ states was determined [38], where the main source of uncertainty was due to the ratio of the branching ratios $K^\pm \rightarrow \pi^\pm \pi^- \pi^+$ and $K^\pm \rightarrow \pi^\pm \pi^0 \pi^0$.

The new measurement performed at KLOE [39] is based on the two samples selected with the usage of $K^\pm \rightarrow \mu^\pm \nu (\gamma)$ ($K_{\mu 2}$ tags) and $K^\pm \rightarrow \pi^\pm \pi^0 (\gamma)$ ($K_{\pi 2}$ tags) events. These independent samples of pure kaons for the signal selection are useful for systematic uncertainties evaluation and cross-checks [40]. The above mentioned decays are identified from the momentum of the charged secondary track in the kaon rest frame evaluated using the pion mass hypothesis, the selection efficiency of the two tagging normalization samples are similar and about 36%. In order to reduce influence of the trigger efficiency on the signal side, a normalization sample of $K_{\mu 2}$ or $K_{\pi 2}$ tags is selected. In addition K^- is used as the tagging kaon ($K_{\mu 2}$ or $K_{\pi 2}$) and K^+ as the tagged kaon (signal) due to a factor of $\sim 10^3$ lower nuclear cross section for positive kaons with momenta $\sim 100 \text{ MeV}$ with respect to that of negative kaons [41].

To evaluate the momentum of the tagged kaon at the interaction point (IP) the momentum of the tagging kaon at the IP (backward extrapolated from its first hit in the drift chamber (DC)) and the momentum of the ϕ -meson measured run by run with Bhabha scattering events are used. Then momentum of K^+ is extrapolated inside the DC (path of the signal kaon). Requirement of the position of K^+ decay vertex inside inner radius of the drift chamber is applied in order to decrease number of charged track in the DC, since both kaon and pions have momenta lower than $\sim 200 \text{ MeV}$ and therefore curl up in the KLOE magnetic field, which increases the number of tracks reconstructed with low quality. Additionally only two of the pion tracks are reconstructed to search for a vertex along the signal kaon path.

The number of $K^+ \rightarrow \pi^+ \pi^- \pi^+ (\gamma)$ is extracted from the comparison of the MC-predicted shapes for

the signal and the background and the experimental missing mass spectrum $m_{miss}^2 = E_{miss}^2 - (\vec{p}_{K^+} - \vec{p}_1 - \vec{p}_2)^2$ where \vec{p}_1 and \vec{p}_2 are the momenta of the selected tracks.

The branching ratio is given by:

$$BR(K^+ \rightarrow \pi^+\pi^-\pi^+(\gamma)) = \frac{N_{K \rightarrow 3\pi}}{N_{tag}} \times \frac{1}{\epsilon} \quad (4)$$

where $N_{K \rightarrow 3\pi}$ is the number of signal events, N_{tag} is the number of tagged events and ϵ is the overall signal selection efficiency (detector acceptance, reconstruction efficiency, tag bias, corrections for the machine and cosmic-ray background).

The effect of the influence of the charged kaon lifetime through the detector acceptance on the $BR(K^+ \rightarrow \pi^+\pi^-\pi^+(\gamma))$ was also evaluated based on the MC simulation and then applied as a weight to the MC events, both for the signal and the control sample selection procedures.

Averaging two results for $K^- \rightarrow \mu^-\bar{\nu}(\gamma)$ and $K^- \rightarrow \pi^-\pi^0(\gamma)$ samples, accounting for correlations, the final result of the measurement is [39]:

$$BR(K^+ \rightarrow \pi^+\pi^-\pi^+(\gamma)) = (55.65 \pm 0.31_{sta} \pm 0.25_{sys}) 10^{-3}$$

which is fully inclusive of final-state radiation and has a 0.72% accuracy, which makes it a factor $\simeq 5$ better with respect to the previous direct measurement [29]. The PDG [30] value, obtained from a constrained fit is:

$$BR(K^+ \rightarrow \pi^+\pi^-\pi^+(\gamma)) = (55.9 \pm 0.4) 10^{-3}.$$

4.3. Dark forces searches

A series of recent astrophysical observations have obtained results which cannot be explained within the framework of the Standard Model (SM) [42, 43, 44, 45, 46, 47, 48] and [49, 50, 51, 52]. Several dark matter models have been proposed to explain these anomalies. In particular a new gauge interaction would be mediated by a new massive vector gauge boson, the U boson (dark photon), which could kinetically mix with the SM hypercharge (ordinary photon). The mass of the U boson is expected to be less than two proton masses to avoid effects, not observed, to the anti-proton astrophysical flux. This small coupling between dark matter and the SM can be described by a single kinetic mixing parameter: $\epsilon (= \alpha_D/\alpha_{EW})$. The resulting Lagrangian would be:

$$\mathcal{L}_{mix} = -\frac{\epsilon}{2} F_{\mu\nu}^{EW} F_{Dark}^{\mu\nu}$$

The U bosons should be observed as a sharp resonance at m_U in the invariant-mass distributions of final-state

charged lepton or pion pairs in reactions of the type $e^+e^- \rightarrow U\gamma$ with $U \rightarrow X^+X^-$ ($X = e/\mu/\pi$) or in meson Dalitz decays.

In Ref. [53] Φ decay like $\Phi \rightarrow \eta U$ with $U \rightarrow e^+e^-$ are proposed. At KLOE two different searches were performed using the decay chain $\Phi \rightarrow \eta U$ with $U \rightarrow e^+e^-$ and $\eta \rightarrow \pi^+\pi^-\pi^0$ [54] and $\eta \rightarrow \pi^0\pi^0\pi^0$ [55]. The two analyses selected a final sample of ~ 13000 and ~ 31000 events, respectively, using 1.7 fb^{-1} of data. Irreducible background from Dalitz decay $\Phi \rightarrow \eta e^+e^-$ was simulated in the assumption of VMD models [56]. A resonant peak was not observed and the CLS technique was used to set an upper limit on the strength of kinetic mixing parameter as a function of U boson mass [57]. The 90% confidence level limit is shown in fig. 6.

Using 239.3 pb^{-1} of data collected in 2002 a search for U boson in the process $e^+e^- \rightarrow U\mu^+\mu^-$ has been performed [58]. The signal would appear as a narrow resonance in the final state dilepton invariant-mass spectrum. For this analysis the two charged tracks are required to be emitted at large-angle such that their energy is deposited in the barrel of the calorimeter. The initial-state radiation (ISR) photon was not explicitly detected, being emitted at small angle with respect to the beam axis, where its direction was reconstructed using kinematics of the charged leptons. The signal selection is performed by using a variable called the track mass, m_{track} , that was computed using energy and momentum conservation, assuming two equal-mass oppositely-charged final-state particles and one unobserved photon. The final invariant mass spectrum was obtained after subtracting residual background and correcting for efficiency and luminosity. No resonant peak was observed so the CLS technique was used to estimate the maximum number of U boson signal events that can be excluded at 90% confidence level, N_{CLS} . In the estimate a systematic uncertainty of $\sim 1.5\%$ has been taken into account. From N_{CLS} is possible to estimate a limit on the kinetic mixing parameter:

$$\epsilon(m_{\mu\mu}) = \frac{\alpha_D}{\alpha_{EW}} = \frac{N_{CLS}(m_{\mu\mu})}{\epsilon_{eff}(m_{\mu\mu})} \frac{1}{H(m_{\mu\mu})I(m_{\mu\mu})\mathcal{L}_{int}} \quad (5)$$

where the radiator function, $H(m_{\mu\mu})$, was evaluated with MC dedicated simulation based on PHOKARA and $\mathcal{L}_{int} = 239.3 \text{ pb}^{-1}$ is the integrated luminosity and $\epsilon_{eff}(m_{\mu\mu})$ ranges between 1%-10%. The 90% confidence level limit is shown in fig. 6.

The search of $U \rightarrow \mu^+\mu^-$ is obviously limited to U boson masses with $m_U > 2m_\mu$. To scan for lower values a search in the e^+e^- final state is needed. In this case, to have enough statistics around the threshold ($m_{ee} = 2m_e$), the event selection has been performed by selecting the ISR photon and leptons emitted at large angle (detected in the

barrel). The resulting background contamination was less than 1.5%. No resonant U boson peak was observed prompting another use of the CLS technique to estimate N_{CLS} , the number of U boson signal events excluded at 90% confidence level. We used eq. 5 with $m_{\mu\mu} \rightarrow m_{ee}$ to set a preliminary limit on the kinetic mixing parameter as a function of m_U . For this analysis ε_{eff} ranges between 1.5% and 2.5%, and the $\mathcal{L}_{int} = 1.54 \text{ fb}^{-1}$ from 2004-05 KLOE data. Results are shown in fig. 6

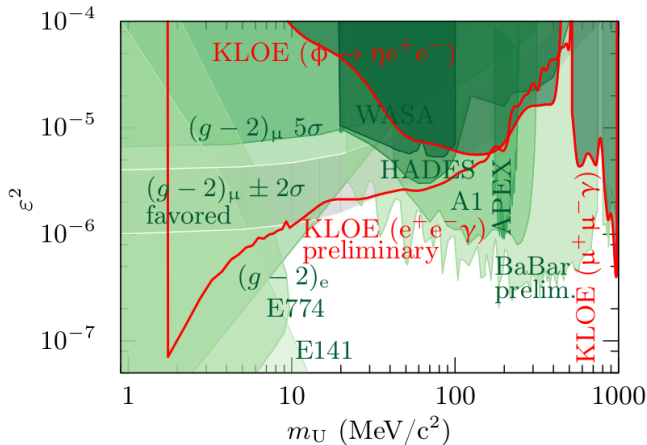


Figure 6. Summary of 90% CL exclusion limits on the dark sector coupling as a function of the U boson invariant mass.

At KLOE it has been investigated also a scenario in which the hidden symmetry is spontaneously broken by a Higgs-like mechanism, thus implying the existence of at least one other scalar particle, h' . The hypothetical dark Higgs-strahlung process $e^+e^- \rightarrow Uh'$ with $U \rightarrow \mu\mu$ has been investigated using KLOE data. The main advantage of this process is that is suppressed by a single factor of ϵ instead of ϵ^2 as for the process already described. The obvious implication of that is the possibility to set stricter limits with same amount of statistics. The production cross section of this process would be proportional to the product of the dark coupling and the kinetic mixing strength $\alpha_D \times \epsilon^2$ [60]. Assuming $m_{h'} < m_U$ the dark Higgs boson would have a large lifetime escaping the KLOE detector without interacting. KLOE has performed this analysis using 1.65 fb^{-1} of data collected with center-of-mass collision energy at the Φ -peak, and 0.2 fb^{-1} of data with a center-of-mass energy of 1000 MeV. Mass resolutions were found to be 1 MeV for $m_{\mu\mu}$ (m_U) and 10 MeV for the missing mass ($m_{h'}$). The signature of the dark Higgs-strahlung process would be a sharp peak in the two-dimensional distribution missing mass versus $m_{\mu\mu}$. The binning has been chosen such that 90-95% of the signal would be in a single bin. The evaluation of background has been performed

using a sliding 5×5 bin matrix (excluding the central bin) to determine background MC simulation scale factors. The selection efficiency was evaluated using MC simulations and varied between 15% and 25%. A conservative estimate of 10% systematic contribution has been considered. No evidence of the dark Higgs-strahlung process was found. Using uniform prior distributions, 90% confidence level Bayesian upper limits on the number of events, $N_{90\%}$, were derived separately for the two samples used. The results were then converted in terms of the dark Higgs-strahlung production cross section parameters:

$$\alpha_D \times \epsilon^2 = \frac{N_{90\%}}{\varepsilon_{eff}} \frac{1}{\sigma_{Uh'}(\alpha_D \epsilon^2 = 1) \cdot \mathcal{L}_{int}}$$

where \mathcal{L}_{int} is the integrated luminosity and

$$\sigma_{Uh'} \propto \frac{1}{s(1 - m_U^2/s)^2}$$

is the total cross section evaluated in the assumption $\alpha_D \epsilon^2 = 1$. The combined 90% confidence level limits from on- and off-peak data are shown fig. 7 as projections onto $m_{\mu\mu}$.

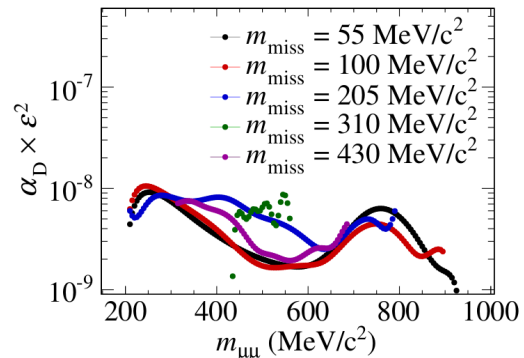


Figure 7. Limits from dark Higgs-strahlung process.

5. Conclusions

DAΦNE commissioning has been delayed by several external faults, but several clear results have been achieved in terms of instantaneous luminosity and beam currents. Limiting factors to achieve the desired goal of $3 \text{ fb}^{-1}/\text{year}$ integrated luminosity have been investigated and several knobs still have to be used to fully exploit DAΦNE capability. KLOE-2 detector commissioning is ongoing and the collaboration is quite confident to be able to start data taking during next months. Performance of new detectors as well as the old one are as expected. The KLOE-2 collaboration is still exploiting the old KLOE dataset producing several

interesting physics results. The new dataset will be of great importance to improve and complete several KLOE measurements especially on the $\gamma\gamma$ physics and kaon interferometry.

6. References

- [1] G. Vignola et al., Frascati Phys. Ser. 4:19-30, 1996.
- [2] P. Raimondi et al., arXiv:physics/0702033; C. Milardi et al., Int.J.Mod.Phys.A24:360-368, 2009; M. Zobov et al., Phys. Rev. Lett. 104, 174801 (2010).
- [3] C. Milardi et al 2012 JINST 7 T03002.
- [4] C. Milardi et al, IPAC10 p. 1527; C. Milardi et al,IPAC11, p. 3687.
- [5] G. Amelino-Camelia et al., EPJC 68 619.
- [6] C. Milardi et al, THPRI002, IPAC14 .
- [7] A. De Santis et al, THPRI015, IPAC14.
- [8] C. Milardi et al, WEOCA03, IPAC14 .
- [9] D. Alesini et al., IPAC10, p. 1515.
- [10] D. Alesini et al., Phys.Rev.Lett. 110, 124801 (2013).
- [11] D. Shatilov, A. Valishev, private communication.
- [12] A. Drago et al., PAC05, p. 1841; A. Drago et al.,IPAC11, p. 490.
- [13] A. Drago, <http://indico.cern.ch/event/306551/>.
- [14] M. Adinolfi *et al.*, KLOE Coll., Nucl. Instr. Meth. A 488 (2002) 51.
- [15] M. Adinolfi *et al.*, KLOE Coll., Nucl. Instr. Meth. A 482 (2002) 363.
- [16] G. Amelino-Camelia *et al.*, Eur. Phys. J. C **68** (2010) 619 [arXiv:1003.3868 [hep-ex]].
- [17] C. Milardi *et al.*, DAFNE Collaboration, arXiv:1006.1487.
- [18] D. Babusci *et al.*, Nucl. Instrum. Meth. A **617**, 81 (2010).
- [19] F. Archilli, *et al.*, Nucl. Instrum. Meth. A **617** (2010) 266.
- [20] F. Happacher *et al.*, Nucl. Phys. Proc. Suppl. **197**, 215 (2009).
- [21] M. Cordelli *et al.*, Nucl. Instrum. Meth. A **617**, 105 (2010).
- [22] A. Balla, *et al.*, Nucl. Instrum. Meth. A **628** (2011) 194 [arXiv:1003.3770 [physics.ins-det]].
- [23] A. Di Domenico,
- [24] A. Einstein, B. Podolsky and N. Rosen, Phys. Rev. **47**, 777 (1935).
- [25] V. A. Kostelecky, Phys. Rev. D **64** (2001) 076001 [hep-ph/0104120].
- [26] O. W. Greenberg, Phys. Rev. Lett. **89** (2002) 231602.
- [27] F. Ambrosino *et al.* [KLOE Coll.], Phys. Lett. B **642** (2006) 315 [hep-ex/0607027].
- [28] D. Babusci *et al.* [KLOE-2 Collaboration], Phys. Lett. B **730**, 89 (2014) [arXiv:1312.6818 [hep-ex]].
- [29] I.H. Chiang, *et al.*, Phys. Rev. D **6** (1972) 1254.
- [30] PDG, Phys. Rev. D **86** (2012) 010001.
- [31] W.T. Ford, *et al.*, Phys. Rev. Lett. **25** (1970) 1370.
- [32] NA48 coll., J.R. Batley, *et al.*, Phys. Lett. B **633** (2006) 173.
- [33] P. Budini, L. Fonda, Phys. Rev. Lett. **6** (1961) 419.
- [34] N. Cabibbo, Phys. Rev. Lett. **93** (2004) 121801.
- [35] N. Cabibbo and G. Isidori, JHEP 0503 (2005) 21.
- [36] G. Colangelo, J. Gasser, B. Kubis, A. Rusetsky, Phys. Lett. B **638** (2006) 187.
- [37] M. Bissegger, A. Fuhrer, J. Gasser, B. Kubis, A. Rusetsky, Nucl. Phys. B **806** (2009) 178.
- [38] NA48 coll., J.R. Batley, *et al.*, EPJ B **64** (2009) 589.
- [39] D. Babusci *et al.* [KLOE/KLOE-2 Collaboration], Phys. Lett. B **738** (2014) 128 [arXiv:1407.2028 [hep-ex]].
- [40] KLOE coll., F. Ambrosino, *et al.*, JHEP **02** (2008) 98
- [41] C.B. Dover and G.E. Walker, *The interaction of kaons with nucleons and nuclei*, Physics Report, **89** 1-177 (1982).
- [42] O. Adriani, et al., Nature 458 (2009) 607.
- [43] P. Jean, et al., Astron. Astrophys. 407 (2003) L55.
- [44] J. Chang, et al., Nature 456 (2008) 362.
- [45] HESS Collaboration, Phys. Rev. Lett. 101 (2008) 261104.
- [46] HESS Collaboration, Astron. Astrophys. 508 (2009) 561.
- [47] A. A. Abdo, et al., Phys. Rev. Lett. 102 (2009) 181101.
- [48] R. Bernabei, et al., Int. J. Mod. Phys. D 13 (2004) 2127.
- [49] R. Bernabei, et al., Eur. Phys. J. C 56 (2008) 333.
- [50] CoGeNT Collaboration, Phys. Rev. Lett. 106 (2011) 131301.
- [51] CoGeNT Collaboration, Phys. Rev. Lett. 107 (2011) 141301.
- [52] AMS Collaboration, Phys. Rev. Lett. 110 (2013) 141102.
- [53] M. Reece, L. T. Wang, JHEP 07 (2009) 51.
- [54] KLOE-2 Collaboration, Phys. Lett. B 706 (2012) 251255.
- [55] KLOE-2 Collaboration, Phys. Lett. B 720 (2013) 111115.
- [56] L. G. Landsberg, Phys. Rep. 128 (1985) 301.
- [57] G. C. Feldman, R. D. Cousins, Phys. Rev. D 57 (1998) 3873.
- [58] KLOE-2 Collaboration, Phys. Lett. B 736 (2014) 459464.
- [59] L. Barz'e, et al., Eur. Phys. J. C 71 (2011) 1680.
- [60] A. R. B. Batell, M. Pospelov, Phys. Rev. D 79 (2009) 115008.